

Exploiting Self-Assembly of Block Copolymers to Fabricate Nanocomposite Thin Films with Controlled Morphology at Nanoscale

Anna Malafronte^{a,*}, Alessandro Emendato^a, Finizia Auriemma^a, Rocco Di Girolamo^a, Michele Laus^b, Federico Ferrarese Lupi^c, Claudio De Rosa^a

^aDipartimento di Scienze Chimiche, Università degli Studi di Napoli Federico II, Complesso Monte S. Angelo, Via Cintia, 80126, Napoli, Italy.

^bDipartimento di Scienze e Innovazione Tecnologica (DISIT), Università Del Piemonte Orientale A. Avogadro, Viale T. Michel 11, 1512, Alessandria, Italy.

^cDivisione di Metrologia Dei Materiali Innovativi e Scienze Della Vita, Istituto Nazionale di Ricerca Metrologica, Strada Delle Cacce 91, 10135, Torino, Italy.
anna.malafronte@unina.it

As the advantageous properties of nanoparticles (NPs) often emerge only when appropriate coupling and exchange phenomena between the NPs can take place, the control of the inter-particle distance, regular ordering, and location of the nanoparticles onto solid supports is a critical issue. A robust method to control the spatial organization of NPs onto solid supports, based on the use of self-assembling di-block copolymers (BCPs) as structure-guiding material, is reported. Two different polystyrene-*b*-poly(methyl methacrylate) (PS-*b*-PMMA) BCPs, characterized by a different PS volume fraction, were used as matrices for the fabrication of nanocomposite thin films with cylindrical and lamellar morphologies controlled at the nanoscale. Selective inclusion of surface functionalized gold (Au) and zinc oxide (ZnO) NPs of appropriate size in the PS nanodomains was achieved from dispersions of the BCPs and NPs in a common solvent. The orientation of the BCPs cylinder and lamellar nanodomains in spin-coated thin films was controlled by solvent and thermal annealing protocols, coupled with techniques of surface neutralization.

1. Introduction

The morphological control at nanoscale is a key issue to fully exploit the unique properties of polymers-based composite thin films containing nanoparticles (NPs) (Fu et al., 2019) and linear di-block copolymers (BCPs) represent ideal scaffolds to this aim, since the spontaneous self-assembly of BCPs can be used to control and direct the positioning of the NPs onto solid supports. The self-assembly of BCPs produces periodic nanostructured morphologies in which, depending on their volume fraction, the two different blocks are organized in lamellar, cylindrical, spherical, or inter-connected nanodomains (Bates et al., 1990). The ability to control morphology and size of BCP nanodomains makes these materials particularly attractive as scaffolds to prepare a large number of tailor-made nanostructured materials, such as nanocomposite (Bockstaller et al., 2005) and nanoporous thin films (Auriemma et al., 2017) or templates for nanolithography (Bates et al., 2014). The BCP nanodomains can act as hosts for sequestering ex-situ synthesized NPs of appropriate chemical affinity and dimensions, thus leading to nanocomposites in which the positioning of the NPs is guided by the self-assembly of the BCP matrix. In this perspective, a precise control of the orientation of the nanodomains is also necessary. In particular, the accomplishment of self-assembled BCPs thin films in which the cylindrical and lamellar nanodomains are oriented perpendicularly to the support is highly desired for many applications (Darling, 2007). Thermal and solvent annealing are the simplest and the most commonly used methods to control of the orientation of the BCPs nanodomains (Lazzari et al., 2010). Thermal annealing consists of controlled heating at a temperature above the glass transition (T_g) of the constituent blocks for a specific time. Solvent annealing approach, consisting in exposing the BCP thin film to vapors of a good solvent, instead,

entails an increase in chain mobility by the effect of transient plasticizer of the solvent. The modulation of the interactions between the solid supports and the polymer blocks is obviously also important in thin film configuration. In the case of lamellar BCPs, an efficient method to favour the perpendicular orientation of the nanodomains consists in chemically modifying the support by grafting an appropriate random copolymer brush layer (RCP). The RCP has the role to minimize any tendency of the blocks to establish preferred interactions with the support, so preventing the formation of a parallel orientation of the nanodomains (Darling, 2007). In this work, BCP-based nanocomposites with different morphologies controlled at nanoscale, containing gold (Au) and zinc oxide (ZnO) NPs, were fabricated by using polystyrene-*b*-poly(methyl methacrylate) (PS-*b*-PMMA) block-copolymers as templates. In particular, two different PS-*b*-PMMA BCPs able to self-assemble in cylindrical or lamellar morphologies, named Cyl-PSMMA and Lam-PSMMA, respectively, were used to prepare thin films by spin-coating onto solid supports (glass and indium thin oxide (ITO)-coated slides). The perpendicular orientation of the cylindrical and lamellar nanodomains was obtained by using solvent annealing protocols in the case of the Cyl-PSMMA sample and by grafting a random PS-*r*-PMMA copolymer (RCP) to the ITO supports and followed by thermal annealing in the case of the Lam-PSMMA sample. Organic-capped Au and ZnO NPs were also synthesized, and toluene solutions containing both the NPs and BCPs were prepared. Nanocomposite thin films were obtained by spin coating the toluene solutions onto solid supports (Figure 1). The application of thermal and solvent annealing protocols to the so obtained thin films results in nanocomposites in which the NPs are selectively included in the PS perpendicularly oriented cylindrical and lamellar nanodomains of the BCPs. It is worth to note that Au and ZnO NPs, due to their peculiar properties, are widely investigated for many nanotechnological applications. ZnO is a *n*-type inorganic semiconductor widely used in electronics, optoelectronics, electrochemical and field emission devices, as well as in organic and hybrid solar cells (Özgür et al., 2005). Au NPs find applications ranging from catalysis (Ishida et al., 2020) to biological and/or medical areas (Elahi et al., 2018). The presence of thiol units on the surface of nanoparticles, in addition to favoring the chemical affinity of the NPs with the PS domains of the BCPs, gives the material an electric-field-induced charge transfer mechanism to be exploited for building electronic devices with memory functions (Ouyang et al., 2004).

2. Materials and Methods

2.1 Materials

The PS-*b*-PMMA BCPs (Table 1) were purchased from Polymer Source, Inc. Glass supports and indium thin oxide (ITO)-coated slides were purchased from Carlo Erba Reagents and Delta Technologies, respectively. The surface of the ITO-coated slides were neutralized by grafting a brush layer of ω -hydroxyl terminated poly(styrene-*r*-methyl methacrylate) (RCP, $M_n = 8.10 \text{ kg mol}^{-1}$, styrene fraction = 58.0 (w/w), polydispersity = 1.24), by using the procedure described by Ferrarese Lupi et al. (2014). The ITO supports functionalized with the random copolymer will be indicated as ITO-RCP supports.

2.2 Synthesis and UV-Vis characterization of the nanoparticles (NPs)

Au NPs bearing on the surface 2-naphthylthiolate (NT) units were synthesized using the method described by Brust et al. (1994). ZnO NPs coated with *n*-hexadecylamine (HDA) and *tert*-butylphosphonic acid (TBPA) molecules were synthesized by thermal decomposition of zinc acetate (0.8 mmol) in hot TBPA/HDA (0.5 mmol/0.02 mol) mixture, by using the procedure reported by Cozzoli et al. (2003). Absorption spectra of NPs dispersions in toluene were acquired by using a Cary Varian 5000 equipped with an UV-vis monochromator in the wavelength range 400-800 nm and 290-400 nm for Au NPs and ZnO NPs, respectively, with a resolution of 1 nm.

2.3 Preparation of thin films of the neat BCPs and of the nanocomposites

Thin films (thickness 65-70 nm) of the neat BCPs were prepared by spin coating 1-2 wt% BCPs solutions in toluene onto solid supports, that is glass in the case of the Cyl-PSMMA sample and ITO-RCP supports in the case of Lam-PSMMA copolymer, by using a Laurell ws650-mz-23-npp spin processor. Solvent annealing of the Cyl-PSMMA thin films was performed by exposing the films to vapors of dichloromethane at room temperature for 10 and 20 min. The thermal annealing of the Lam-PSMMA thin films was performed by heating the films at 190 °C, under vacuum, for 6 and 24 hours. Thin films of the nanocomposites consisting of Cyl-PSMMA and Au NPs were prepared by spin coating a toluene solution containing 2 wt% BCP and 0.1 wt% Au NPs onto glass supports, and successive exposure at room temperature to dichloromethane vapors for 20 min. Nanocomposites based on Lam-PSMMA matrix and ZnO NPs were prepared by spin coating a toluene solution containing 1 wt% BCP and 0.1 wt% ZnO NPs onto ITO-RCP supports, and successive thermal annealing in vacuum at 190 °C per 24 h. A scheme of spin-coating method used to prepare the nanocomposites is reported in Figure 1.

2.4 Transmission electron microscopy (TEM) characterization

TEM images were acquired in bright field mode using a FEI Tecnai G2 200 kV Transmission Electron Microscope and a Philips EM 208S TEM with an accelerating voltage of 200 kV or 120 kV. Small sections of the carbon-coated films were floated off onto distilled water and picked up by 200 mesh TEM copper grids. Samples of NPs for TEM analysis were prepared by casting a drop of diluted dispersions ($0.5 - 1 \text{ mg mL}^{-1}$) of the NPs in toluene on the surface of a carbon-coated TEM copper grid. In order to achieve a good contrast between PS and PMMA nanodomains, some films were stained with ruthenium tetroxide (RuO_4) by exposition of the TEM grids to RuO_4 vapors at room temperature. The size of the NPs, the dimensions of the PS and PMMA nanodomains and the inter-domain spacing were calculated from the TEM images by using ImageJ software (National Institutes of Health, available free of charge at Web site rsb.info.nih.gov/ij/). At least 200 independent measurements were taken at different locations of the TEM images of the samples.

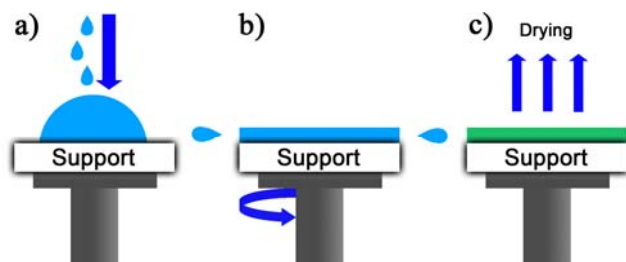


Figure 1: Scheme of spin-coating method used to prepare the nanocomposites: (a) few drops of toluene solution containing the BCP and NPs were deposited onto solid supports (glass or ITO-RCP supports); (b) the rotation at high spinning speed drove the solvent radically outward; (c) the complete evaporation of the solvent produced thin and uniform nanocomposite films; the morphology of the nanocomposite thin films was optimized by solvent or thermal annealing.

3. Results and discussion

3.1 Preparation and morphology optimization of thin films of neat BCPs

Two different polystyrene-*b*-poly(methyl methacrylate) BCPs, named Cyl-PSMMA and Lam-PSMMA (Table 1), were used as scaffolds for the preparation of nanocomposites. The volume fraction of the PS block in the BCPs (f_{PS}) was selected to obtain a cylindrical microphase-separated morphology, in which the PS blocks form a hexagonal array of cylinders in the PMMA matrix ($f_{\text{PS}} = 0.28$, sample Cyl-PSMMA), or a lamellar morphology ($f_{\text{PS}} = 0.52$, sample Lam-PSMMA). The first step of this work consisted in setting up a robust and reproducible procedure to obtain nanostructured thin films of the BCPs (Table 1) characterized by a perpendicular orientation of the PS cylindrical nanodomains (for the Cyl-PSMMA sample) and of the lamellar PS and PMMA nanodomains (for the Lam-PSMMA sample).

Table 1: Average molar mass (M_n) of the PS and PMMA blocks, polydispersity index ($\mathcal{D}=M_w/M_n$) and volume fraction of the PS block (f_{PS}) of the two PS-*b*-PMMA BCPs (named Cyl-PSMMA and Lam-PSMMA) used in this work.

Sample name	M_n (PS) (kg mol^{-1})	M_n (PMMA) (kg mol^{-1})	\mathcal{D}	f_{PS}
Cyl-PSMMA	47.4	140.4	1.11	0.28
Lam-PSMMA	25.0	26.0	1.06	0.52

A representative bright-field TEM image of RuO_4 -stained thin films (thickness 65 nm) of Cyl-PSMMA, prepared by spin coating a 2 wt% BCP toluene solution onto glass supports, is reported in Figure 2a. The dark regions correspond to the stained PS cylindrical nanodomains that appear disorderly dispersed in the PMMA matrix (lighter regions in Figure 2a). The Cyl-PSMMA thin film of Figure 2a was exposed to vapors of dichloromethane, which has a good affinity for both PS and PMMA blocks, to obtain a perpendicular orientation of PS cylinders (i.e., axes of the cylinders normal to the support). After an exposure time of 10 min (Figure 2a') a mixed orientation of the PS cylindrical domains is observed. By increasing the solvent annealing time up to 20 min (Figure 2a'') a high degree of perpendicular orientation of PS cylinders was achieved. A good lateral ordering in the hexagonal packing of PS cylinders was obtained. The mean PS inter-domain spacing was approximately 60 nm, whereas the average diameter of the PS domains was 30-35 nm. A bright-

field TEM image of RuO₄-stained thin films of Lam-PSMMA (thickness 70 nm), prepared by spin-coating the toluene solution onto ITO-RCP supports, is reported in Figure 2b. No phase separation is observed by simply spin coating the thin films. Thermal annealing treatments are necessary in order to provide sufficient mobility to the polymer chains to promote the phase separation and orientation of the nanodomains. In particular, after annealing at 190 °C for 24 h (Figure 2b''), a disordered lamellar morphology with lamellar domains oriented perpendicular to the support is observed. The vertical orientation of lamellae demonstrates the efficiency of thermal annealing in controlling the nanofeature orientation of the BCPs deposited on ITO supports neutralized with the random PS-*r*-PMMA copolymer (ITO-RCP supports). It is worth to note that the thermal annealing was performed at a temperature higher than the *T*_gs of both PS and PMMA blocks, equal to ≈ 108 and ≈ 130 °C, respectively. The average width of the lamellar PS and PMMA domains, evaluated from the TEM image of Figure 2b'', is ≈ 19 and ≈ 9 nm, respectively. These data indicate that nanostructured thin films of neat BCPs with a well-defined morphology characterized by a perpendicular orientation of the PS cylinder (Figure 2a'') and lamellar (Figure 2b'') nanodomains can be obtained by simple solvent and thermal annealing treatments (Figure 2a and Figure 2b).

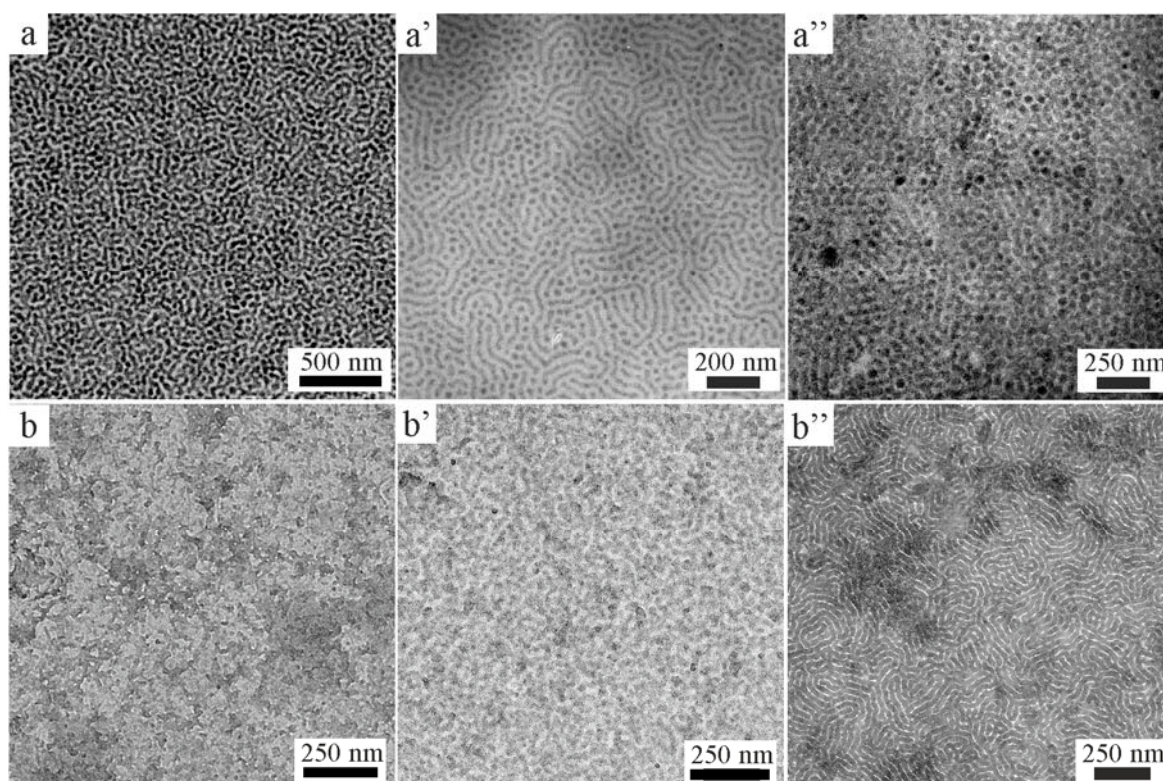


Figure 2: Bright-field TEM images of RuO₄-stained thin films of neat BCPs prepared by spin-coating. Cyl-PSMMA thin films before (a) and after exposition to vapours of dichloromethane for 10 (a') and 20 (a'') min; Lam-PSMMA thin films before (b) and after thermal annealing at 190°C for 6 (b') and 24 (b'') hours.

3.2 Synthesis and Characterization of Au and ZnO nanoparticles

Au NPs bearing on the surface 2-naphthylthiolate (NT) units were prepared according to the procedure described by Brust et al. (1994). The strategy consisted in growing the metallic clusters with the simultaneous attachment of self-assembled thiol monolayers on the growing nuclei. The particles were grown in a two-phase system, in order to allow the surface reaction to take place during metal nucleation and growth. ZnO nanoparticles capped with *n*-hexadecylamine (HDA) and *tert*-butylphosphonic acid (TBPA) were synthesized by using the solution-phase strategy reported by Cozzoli et al. (2003), based on the thermal decomposition of a zinc precursor (zinc acetate) in hot coordinating solvents (TBPA/HDA mixture). The synthesis methods and the coordinating agents were purposely selected in order to obtain nanoparticles of suitable size to be included in the PS nanodomains of the BCPs, to improve chemical affinity with the target PS nanodomains and to favour the dispersion of the NPs in apolar media. This latter aspect is advantageous for the subsequent preparation of the nanocomposites, since a common organic solvent (toluene) has to be used to disperse both

BCPs and NPs. The bright-field TEM images of the synthesized Au and ZnO NPs are reported in Figures 3a and b, respectively. The NPs exhibit a nearly spherical shape, and average diameters of 2.9 ± 0.8 and 5.7 ± 0.9 nm were evaluated for Au and ZnO nanoparticles, respectively. A relative amount of the two ligands HDA:TBPA covering the ZnO NPs surface equal to 1:0.6 was estimated by ^1H NMR experiments (data not shown). Absorption spectra of Au and ZnO NPs dispersions in toluene are reported in Figures 3c and d, respectively. The Au NPs show a surface plasmon peak at ≈ 512 nm (Figure 3c), in agreement with the experimental data obtained for NPs of similar diameter, due to the pronounced increase in the ratio of surface atoms to bulk atoms (Haiss et al., 2007). The absorption spectrum of ZnO NPs (Figure 3d) shows a quite steep onset, indicating a narrow size distribution. The band edge absorption peak appears at ≈ 332 nm. As expected, the position of the peak is blue-shifted with respect to the bulk material (373 nm) (Cozzoli et al., 2003).

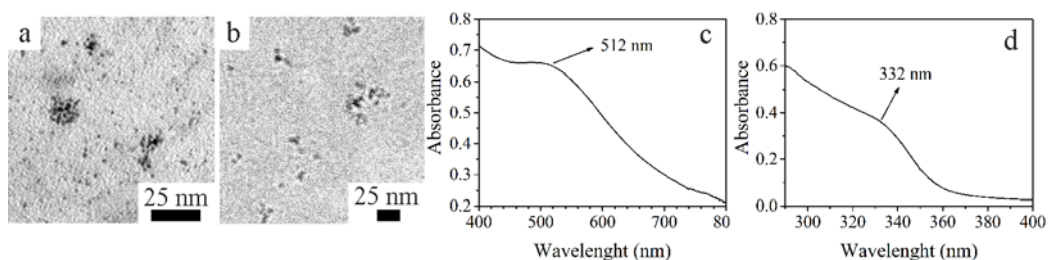


Figure 3: Bright-field TEM images (a, b) and UV-Vis toluene solutions spectra (c, d) of Au (a, c) and ZnO (b, d) NPs.

3.3. Preparation and Characterization of the nanocomposites

BCPs-based nanocomposites containing Au and ZnO NPs were obtained by dispersing the NPs and BCP in a common solvent (toluene), followed by the preparation of the thin films onto solid supports and final solvent or thermal annealing treatments, adopting the best procedures identified for the neat thin films (Figure 2a'' and Figure 2b''). A Bright-field TEM image of a thin film of the nanocomposite consisting of Cyl-PSMMA and Au NPs, prepared by spin coating a toluene solution containing BCP and Au NPs onto glass support and successive exposition at room temperature to dichloromethane vapors for 20 min, is reported in Figure 4a.

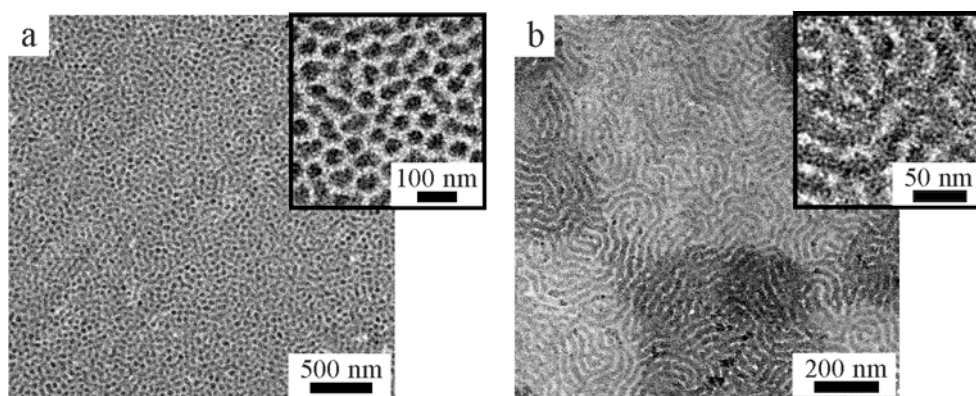


Figure 4: Bright-field TEM images of not-stained Cyl-PSMMA/Au (a) and RuO_4 -stained Lam-PMMA/ZnO (b) nanocomposites thin films. Magnifications are reported in the insets.

Thanks to the solvent annealing procedure, a high degree of perpendicular orientation of PS cylinders over large areas is observed (Figure 4a), in agreement with the results obtained in the case of neat BCP (Figure 2a''). The image of the nanocomposite Cyl-PSMMA/Au NPs (Figure 4a) was acquired without resorting to any staining procedure. The high contrast of dark PS cylinders with respect to the PMMA matrix is due to the selective inclusion of the Au NPs in the PS cylinders (Figure 4a). The selective and uniform inclusion of Au NPs in the target PS cylinders is clearly visible in the magnification of the TEM image reported in the inset of Figure 4a. Interestingly, the pseudo-hexagonal organization of the perpendicularly oriented PS cylinders is retained after the inclusion of the NPs (Figure 4a). The average diameter of PS cylinders in Figure 4a is ≈ 40 nm and their average distance is ≈ 65 nm. These values are only slightly higher than those estimated in the

BCP not filled with Au NPs (Figure 2a''). Bright-field TEM image of a thin film of the nanocomposite consisting of Lam-PSMMA and ZnO NPs, prepared by spin coating a toluene solution containing the BCP and ZnO NPs onto ITO-RCP support, and successive thermal annealing at 190 °C for 24 h, is reported in Figure 4b. A disordered lamellar morphology with the vertical orientation of the lamellar domains is observed (Figure 4b), as for the neat BCP (Figure 2b''). The image (Figure 4b) indicates that ZnO nanoparticles are not dispersed in the whole BCP, but are selectively included in the lamellar RuO₄-stained PS nanodomains. The nanoparticles filling the PS blocks are clearly visible in the inset of Figure 4b. The thermal annealing at a temperature above the T_g s of the PS and PMMA blocks triggers the migration of the ZnO NPs in the PS lamellar domains and simultaneously leads to the formation of the desired vertical morphology of the lamellar BCP domains. The uniform inclusion of Au and ZnO NPs in the target PS domains is achieved thanks to the designed chemical modification of the nanoparticles surface.

4. Conclusions

The method of ex-situ synthesis of organic-capped NPs and successive co-assembly of nanoparticles and BCPs was used to fabricate nanocomposites thin films characterized by a controlled spatial positioning of the guest NPs. In particular, organic-capped Au and ZnO NPs were selectively included in the PS cylinder and lamellar nanodomains of PS-*b*-PMMA copolymers. Solvent and thermal annealing protocols were used to obtain a perpendicular orientation of the PS nanodomains hosting the NPs. The positioning of the guest NPs in the final nanocomposites is guided by the ordering and self-assembly of the host BCP. A hierarchical assembly of organic-inorganic nanostructures, in which one level of self-assembly guides the next, was obtained with the employed method, confirming the possibility to use BCPs as scaffolds for the engineering of nanomaterials with controlled morphology at nanoscale.

References

- Auriemma F., De Rosa C., Malafronte A., Di Girolamo R., Santillo C., Gerelli Y., Fragneto G., Barker R., Pavone V., Maglio O., Lombardi A., 2017, Nano-in-nano approach for enzyme immobilization based on block copolymers, *ACS Applied Materials & Interfaces*, 9, 29318.
- Bates C. M., Maher M. J., Janes D. W., Ellison C. J., Willson C. G., 2014, Block Copolymer Lithography *Macromolecules*, 47, 2 - 12.
- Bockstaller M.R., Mickiewicz R.A., Thomas E.L., 2005, Block copolymer nanocomposites: perspectives for tailored functional materials, *Advanced Materials*, 17, 1331 - 1349.
- Brust M., Walker M., Bethell D., Schiffrin D. J., Whyman R., 1994, Synthesis of Thiol-derivatised Gold Nanoparticles in a Two-phase Liquid-Liquid System, *Journal of the Chemical Society, Chemical Communications*, 7, 801 - 802.
- Cozzoli P. D., Curri M. L., Agostiano A., Leo G., Lomascolo M., 2003, ZnO nanocrystals by a non-hydrolytic route: synthesis and characterization, *The Journal of Physical Chemistry B*, 107, 4756 - 4762.
- Darling S. B., 2007, Directing the self-assembly of block copolymers, *Progress in Polymer Science*, 32, 1152 - 1204.
- Elahi N., Kamali M., Baghersad M. H., 2018, Recent biomedical applications of gold nanoparticles: A review, *Talanta*, 184, 537 – 556.
- Ferrarese Lupi F., Giammaria T. J., Seguini G., Ceresoli M., Perego M., Antonoli D., Gianotti V., Sparnacci K., Laus M., 2014, Flash grafting of functional random copolymers for surface neutralization, *Journal of Materials Chemistry C*, 2, 4909 - 4917.
- Fu S., Sun Z., Huang P., Li Y., Hu N., 2019, Some basic aspects of polymer nanocomposites: A critical review, *Nano Materials Science*, 1, 2 - 30.
- Haiss W., Thanh N. T. K., Aveyard J., Fernig D. G., 2007, Determination of Size and Concentration of Gold Nanoparticles from UV-Vis Spectra, *Analytical Chemistry*, 79, 4215 - 4221.
- Lazzari M., De Rosa C., 2010, Comprehensive Approach to the Alignment and Ordering of Block Copolymer Morphologies, Chapter In: Kurt E. Geckeler and Hiroyuki Nishide (Eds.), *Advanced Nanomaterials*, Wiley-VCH Verlag GmbH & Co. KGaA, 111 - 158.
- Ishida T., Murayama T., Taketosh A., Haruta M., 2020, Importance of Size and Contact Structure of Gold Nanoparticles for the Genesis of Unique Catalytic Processes, *Chemical Reviews*, 120, 464 - 525.
- Mai Y., Eisenberg A., 2012, Self-assembly of block copolymers, *Chemical Society Reviews*, 41, 5969 – 5985.
- Ouyang J., Chu C.-W., Szmanda C. R., Ma L., Yang Y., 2004, Programmable polymer thin film and non-volatile memory device, *Nature Materials*, 3, 918 - 922.
- Özgür Ü., Alivov Ya. I., Liu C., Teke A., Reshchikov M. A., Doğan S., Avrutin V., Cho S.-J., Morkoç H., 2005, A comprehensive review of ZnO materials and devices. *Journal of Applied Physics*, 98, 041301.